

REPORT



C_{H2} domain orientation of human immunoglobulin G in solution: Structural comparison of glycosylated and aglycosylated Fc regions using small-angle X-ray scattering

Seiki Yageta^{a,b,c}, Hiroshi Imamura^{id a,d}, Risa Shibuya^{id b}, and Shinya Honda^{id a,b,c}

^aBiomedical Research Institute, National Institute of Advanced Industrial Science and Technology (AIST), Tsukuba, Ibaraki, Japan; ^bDepartment of Computational Biology and Medical Sciences, Graduate School of Frontier Sciences, the University of Tokyo, Kashiwa, Chiba, Japan; ^cManufacturing Technology Association of Biologics, Tsukuba, Ibaraki, Japan; ^dDepartment of Applied Chemistry, College of Life Sciences, Ritsumeikan University, Kusatsu, Shiga, Japan

ABSTRACT

The *N*-linked glycan in immunoglobulin G is critical for the stability and function of the crystallizable fragment (Fc) region. Alteration of these protein properties upon the removal of the *N*-linked glycan has often been explained by the alteration of the C_{H2} domain orientation in the Fc region. To confirm this hypothesis, we examined the small-angle X-ray scattering (SAXS) profile of the glycosylated Fc region (gFc) and aglycosylated Fc region (aFc) in solution. Conformational characteristics of the C_{H2} domain orientation were validated by comparison with SAXS profiles theoretically calculated from multiple crystal structures of the Fc region with different C_{H2} domain orientations. The reduced chi-square values from the fitting analyses of gFc and aFc associated with the degree of openness or closure of each crystal structure, as determined from the first principal component that partially governed the variation of the C_{H2} domain orientation extracted by a singular value decomposition analysis. For both gFc and aFc, the best-fitted SAXS profiles corresponded to ones calculated based on the crystal structure of gFc that formed a “semi-closed” C_{H2} domain orientation. Collectively, the data indicated that the removal of the *N*-linked glycan only negligibly affected the C_{H2} domain orientation in solution. These findings will guide the development of methodology for the production of highly refined functional Fc variants.

ARTICLE HISTORY

Received 6 July 2018
Revised 24 October 2018
Accepted 31 October 2018

KEYWORDS

Immunoglobulin G; crystallizable fragment region; *N*-linked glycan; singular value decomposition; small-angle X-ray scattering

Introduction

Immunoglobulin G (IgG), the antibody class that is most widely produced for therapeutic purposes,^{1,2} is a large multi-domain protein with an *N*-linked glycan at residue N297 of the C_{H2} domain in the crystallizable fragment (Fc) region. In recent years, therapeutic use of aglycosylated IgG molecules has gained popularity because the lack of glycan is thought to bypass issues with IgG glycan heterogeneity and suppress undesired effector function.^{3–5} Further, aglycosylated IgG molecules can be produced in lower eukaryotes and bacteria, with considerable advantages in terms of short culture time and potential for excellent scale-up in comparison with the conventional IgG generation using mammalian cells.^{6,7} However, it is generally accepted that removal of the *N*-linked glycan from the Fc region affects the properties of the protein, e.g., the stability and function of the Fc region.^{8–14} Any aglycosylated IgG developed as a therapeutic should thus be evaluated to determine the effect of deglycosylation on these properties.

It has long been assumed that removal of the *N*-linked glycan might result in the alteration of the orientation of the C_{H2} domain in the aglycosylated Fc region (aFc).^{15–17} For example, an aFc crystal structure (Protein Data Bank

accession number, PDB: 3S7G) revealed a closed C_{H2} domain orientation, with the two C_{H2} domains more proximal to one another than in the crystal structure of the glycosylated Fc region (gFc) (PDB: 4W4N).^{15,18} In contrast, a recent residual dipolar coupling (RDC) analysis by nuclear magnetic resonance (NMR)¹⁹ examined the C_{H2}-C_{H3} domain orientation in both gFc and aFc in solution, as judged by the relative orientation of each observable N-H bond vector of ¹⁵N-labeled gFc and aFc. The experiment revealed that the C_{H2}-C_{H3} domain orientation in both gFc and aFc is similar to that in a crystal structure of gFc (PDB: 1L6X²⁰). The authors proposed that “the effect of glycosylation on C_{H2} domain orientation is restricted to small amplitudes or small populations”. Their finding suggested the observed perturbation of the C_{H2} domain orientation in the crystal structure of aFc was mainly attributed to the crystal packing forces.²¹

In this study, using small-angle X-ray scattering (SAXS), a powerful tool for the evaluation of protein conformation in solution,²² we proved that the removal of the *N*-glycan only minimally perturbed the C_{H2} domain orientation in aFc in solution. In SAXS, the SAXS profile $I(q)$ is expressed by a Fourier transformation of the pair-distance distribution function $P(r)$, and can also be theoretically calculated if the three-dimensional coordinates of a crystal or modeled protein

CONTACT Shinya Honda  s.honda@aist.go.jp  Biomedical Research Institute, National Institute of Advanced Industrial Science and Technology (AIST), Central 6, 1-1-1 Higashi, Tsukuba, Ibaraki 305-8566, Japan

 Supplemental data for this article can be accessed on the [publisher's website](#).

© 2018 The Author(s). Published with license by Taylor & Francis Group, LLC.

This is an Open Access article distributed under the terms of the Creative Commons Attribution-NonCommercial-NoDerivatives License (<http://creativecommons.org/licenses/by-nc-nd/4.0/>), which permits non-commercial re-use, distribution, and reproduction in any medium, provided the original work is properly cited, and is not altered, transformed, or built upon in any way.

structures are available.²³ Comparison of the experimentally determined and theoretical SAXS profiles validates the protein conformational characteristics in solution. Accordingly, we determined the SAXS profiles of gFc and aFc in a solution at pH 7, and characterized the domain orientation by comparing the experimentally derived profiles with the theoretical SAXS profiles which were calculated using multiple crystal structures and homology modeling.

Results

Measurements of the SAXS profiles

To investigate the conformational characteristics of gFc and aFc in a solution at pH 7, we collected their SAXS profiles (Figure 1). The shapes of gFc and aFc SAXS profiles were similar, but clearly different. The radius of gyration (R_g) and the scattering intensity at zero-angle [$I(0)$] were calculated from the Guinier approximation in the low q region (Figure 1(a) and Table S1). The R_g of gFc and aFc showed slight concentration dependence within the range of 2 to 5 mg/mL of proteins, suggesting weak intermolecular interaction^{24–26} (Figure S1). Therefore, we estimated an interference-free SAXS profiles of gFc and aFc by extrapolating the measured SAXS profiles to an infinite dilution condition (Figure S2).²⁷ R_g from the interference-free SAXS profiles of gFc and aFc was determined to be 26.44 ± 0.31 Å and 28.88 ± 0.31 Å, respectively. Molecular masses estimated from $I(0)$ of gFc and aFc were 53.3 kDa and 50.7 kDa, respectively, which agreed with the molecular masses determined using mass spectrometry (Table S1). Although there was little difference between the raw measured and normalized interference-free SAXS profiles in the small q region (0.005 to 0.05 Å⁻¹), both profiles were employed in further analyses. A Kratky plot [$q^2I(q)$ vs. q] is used to characterize the structural properties of a protein, such as its globularity and flexibility.²⁸ The Kratky plots of gFc and aFc displayed a bell-shaped peak pattern, indicating the formation of a globular structure (Figure 1(b) and Figure S2b). Both plots were obviously bimodal. By using the value of the scattering parameter when the intensity of the Kratky plot is at a maximum (q_m) [i.e., $dq^2I(q)/dq = 0$], R_g can be also estimated from the Guinier approximation, as $\sqrt{3}/q_m$.²⁹ Further, $I(0)$ may be

estimated using the intensity at q_m in the Kratky plot, i.e., $I(0) = [q_m^2I(q_m)]\exp(1)/q_m^2$. R_g and $I(0)$ values of gFc and aFc determined using q_m in the smaller q region of the two peaks ($q_{m,small}$) were close to the R_g and $I(0)$ values determined by the linear fitting of $\ln I(q)$ vs. q^2 (Table S1). These results indicated that gFc had a smaller R_g than aFc despite having a larger molecular mass, which was atypical for globular proteins.

To reveal the origin of the difference in R_g between gFc and aFc, we analyzed a pair-distance distribution function [$P(r)$]. $P(r)$ derived from a Fourier transformation of the SAXS profile provides insight into additional structural properties of a protein in terms of real space (Figure 1(c) and S2d). The $P(r)$ of gFc [$P(r)_{gFc}$] in the 10–60 Å r range was larger than that of aFc [$P(r)_{aFc}$], while $P(r)_{gFc}$ and $P(r)_{aFc}$ agreed with each other in the r ranges of 0–10 Å and 60–100 Å. R_g , calculated as the center of gravity of $P(r)_{gFc}$, was smaller than that of $P(r)_{aFc}$ (Table S1), which was consistent with the result of the Guinier approximation. We interpreted these results as follows. The increased integrated area of $P(r)_{gFc}$ in the 10–60 Å range was derived from the scattering from the N -linked glycan of gFc, and the shift of the center of gravity in $P(r)_{gFc}$ was affected by such increased distance distribution from the N -linked glycan. Moreover, the intra-domain structure and the inter-domain orientations, corresponding to the shortest (0–10 Å) and longest (60–100 Å) distances, respectively, in gFc and aFc were equivalent. This implied that the change of the C_{H2} domain orientation caused by deglycosylation was small. In other words, the removal of the N -linked glycan corresponded to the generation of a hollow sphere from a solid sphere, without altering the size of the outer shell.

To demonstrate the appropriateness of these interpretations, we further evaluated the structural characteristics of gFc and aFc in solution by comparing the experimentally determined SAXS profiles with the theoretical SAXS profiles calculated based on the available crystal structures of gFc and aFc.

Elucidation of attributes that affect the variation among the Fc crystal structures

Due to advances in X-ray crystal structure analysis, a number of Fc crystal structures are now available. These structures exhibit a well known and appreciable variation with respect to

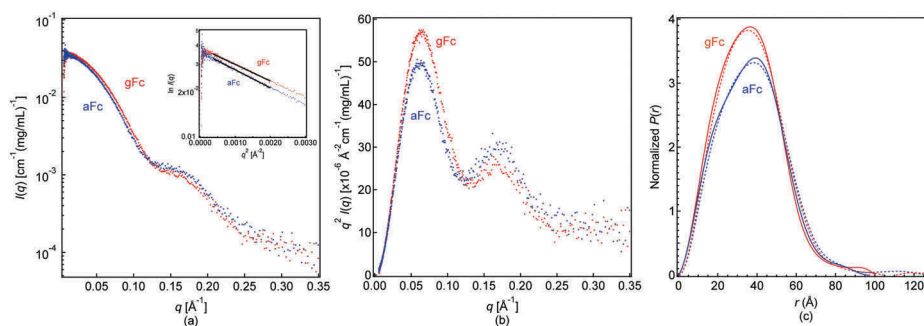


Figure 1. The experimentally determined SAXS profiles of 3 mg/mL protein concentration. q , $I(q)$, r , and $P(r)$ are a scattering parameter, a scattering intensity, a distance between electrons in a particle, and a pair-distance distribution function, respectively (see SUPPLEMENTARY METHOD). The log-linear plot (a) and Kratky plot (b). Inset in (a), Guinier plot. The black straight line indicates the fitted region of the Guinier approximation. The pair-distance distribution function calculated based on the experimentally determined SAXS profiles (c). The dotted and solid lines indicate the direct and indirect Fourier transformation, respectively, of the determined SAXS profiles.

the spatial orientation of the C_{H2} domain, while the C_{H3} domain is well aligned.^{17,30} As a typical example, one aFc crystal structure (PDB: 3S7G) shows a closed C_{H2} domain orientation, in which the C_{H2} domain distance, often determined as the distance between two P238 residues, is relatively small (10.7 Å, measured using Pymol software) compared with that of gFc (e.g., PDB: 4W4N,¹⁸ 19.5 Å), while gFc in complex with Fc gamma receptor (FcγR; e.g., PDB: 4W4O¹⁸) shows an open C_{H2} domain orientation in which the C_{H2} domain distance is relatively large (25.2 Å).

In this study, we first elucidated the intrinsic or extrinsic attributes that affected the variation among the available Fc crystal structures using principal component analysis (PCA). PCA is often used to identify important protein conformations, motions, and noise factors from data with a large number of dependent variables, such as a molecular dynamics trajectory.³¹ Singular value decomposition (SVD), often used in PCA, is a mathematical approach of calculating eigenvalues and eigenvectors from data matrix, and transforming a large number of dependent data variables into a smaller number of independent variables (i.e., principal components), which simplifies the phenomena of interest.³² We performed SVD on a dataset comprising 42 available Fc crystal structures. We extracted the principal components as the attributes independent of each other that intrinsically or extrinsically contributed to the variation between the Fc crystal structures. Each dataset for an individual crystal structure without the N-linked glycan exhibited a deviation from the averaged three-dimensional coordinates of Ca atoms between S239 to S442 when the flexible hinge and C-terminal regions were removed.

The results of SVD are shown in Figure 2. The singular values from the first to seventh components were relatively larger than others. The sum of their contribution ratios was 94.8% (Figure 2(a)). These observations implied that the variation among Fc crystal structures could be mainly described by these seven principal components. The left singular vector from the employed dataset could be interpreted as the direction and magnitude of deviation from the averaged three-dimensional coordinates of each Ca atom, as visualized by a porcupine plot³³ in Figure 2(b) and Figure S3. The first left singular vector showed the direction of the C_{H2} domain

orientation to open or closed orientation from the averaged Ca positions (Figure 2(b)). The left singular vector of the second to seventh principal components described the deviation of the Ca atoms of the C_{H2} domain from the averaged position (Figure S3). We noted that the fifth left singular vector showed a deviation of the C'E loop (Figure S3i). The intrinsic flexibility of this region agreed with the conclusions of previous hydrogen/deuterium exchange mass spectrometry and NMR analyses.^{8,19,34} The magnitude of the right singular vector could be interpreted as weight factor of the left singular vector of each crystal structure (Figure 2(c) and Table S2). For the first principal components, the magnitude of the first right singular vector of each crystal structure correlated with the trends of the open or closed C_{H2} domain orientation compared with the averaged orientation among the 42 crystal structures. For example, the value of the first right singular vector of the crystal structure of aFc (PDB: 3S7G), which typically adopts the closed orientation, was large and negative (−0.399), while it was large and positive (e.g., 0.131 in 4W4O) in the crystal structures of the Fc region in complex with FcγR, which adopts the open orientation. The values of the first right singular vectors of most gFc structures (not in complex) were slightly negative, indicating that they adopted a somewhat closed C_{H2} domain orientation. In this study, we defined the C_{H2} domain orientation of gFc (not in complex) as a "semi-closed" orientation. In gFc in complex with other binding proteins, the value of their first right singular vector varied from negative to positive.

Theoretical SAXS profiles based on crystal structures

To demonstrate the structural similarity between gFc and aFc in solution, we calculated theoretical SAXS profiles based on the individual Fc crystal structures, and fitted these to the experimentally determined SAXS profiles. Evaluation of the characteristics of the best-fitted crystal structure was then confirmed based on the singular vectors deduced from the SVD analysis described above.

We first prepared an intact model structure of gFc and aFc inclusive of the hinge and C-terminal regions by homology modeling. We prepared 80 template structures of gFc and aFc covering the region between S239 to S442 by extracting from

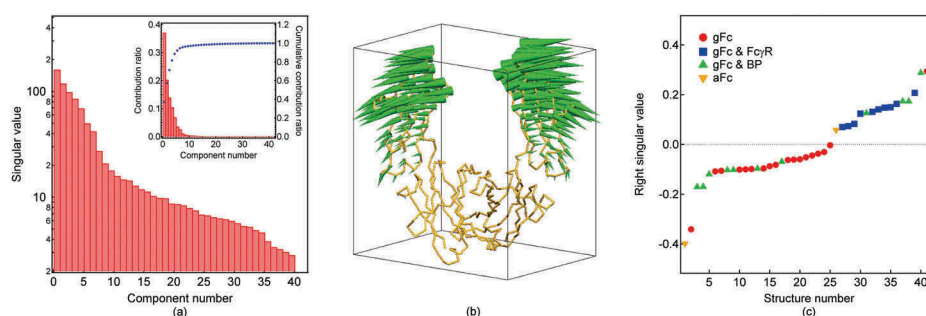


Figure 2. Results of the SVD analysis. The singular value of each component is shown in (a). Inset in (a), the contribution ratio (red bars) and the cumulative contribution ratio (blue dots). The porcupine plots of the first left singular vector are given in (b). The yellow line indicates the averaged three-dimensional coordinates of Ca atoms calculated based on the crystal structure dataset. The green spine indicates the direction and magnitude of the deviation of the first left singular vector from the averaged three-dimensional coordinate of Ca atoms. The first right singular vector of each crystal structure is shown in (c). BP denotes a binding protein such as protein A (See Table S2).

40 crystal structures of the Fc region, and calculated 100 intact model structures from each set of the 80 template structures (Figure 3(a)). As for the *N*-linked glycan coordinates, the rigid coordinates from a specific gFc crystal structure were used as a template (See Materials and Methods section). This was considered reasonable in light of previous SAXS analysis of gFc, in which the *N*-linked glycan was successfully assumed to fill the internal space between C_H2 domains.^{26,35} Then, the SAXS profiles of each intact model structure of gFc and aFc were calculated and fitted to the experimentally determined SAXS profiles at 3 mg/mL protein concentration of gFc and aFc, respectively. The reduced chi-square values from the fitting analysis of 100 intact model structures showed a random-like distribution (Figure S4) because of the conformational difference of the added hinge and C-terminal regions in each intact model structure. Nevertheless, the differences between the reduced chi-square values among the 100 intact model structures were smaller than among the 80 template structures, indicating that the variation of the C_H2 domain orientation affected the shape of SAXS profiles to a greater extent than the conformational variation in the hinge and C-terminal regions. We then extracted a median of the reduced chi-square values of the 100 intact model structures from each of the 80 template structures, and 80 intact median model structures were used as representative model structures.

As shown in Figure 3(b), the reduced chi-square values for 3 mg/mL protein concentration from each representative

model structure of gFc correlated well with those of aFc. We note that the same correlation was also observed in the reduced chi-square values for the interference-free SAXS profiles (Figure S5). This indicated that the presence or absence of the *N*-linked glycan only minimally affected the variation of the goodness of fit, and the difference in the experimentally determined SAXS profiles between gFc and aFc mainly stemmed from the scattering of the *N*-linked glycan in gFc. We next statistically evaluated the goodness of fit and determined the best-fitted representative model structure, by calculating the probability value (*P*-value) using a pair-wise correlation map (CorMap) analysis.³⁶ It should be noted that the reduced chi-square value does not necessarily represent statistical validity because of the difficulty in determining the accurate experimental errors.³⁶ In fact, the propagation of the experimental errors in the processes of calculating the one-dimensional SAXS profiles and averaging the different data frames rendered the experimental errors relatively large, which resulted in quite low reduced chi-square values ($\ll 1.0$, Table S2). When the *P*-values were calculated using the CorMap analysis, most of the representative model structures with higher chi-square values exhibited *P*-values below 0.01, indicating that the null hypothesis (*H*₀) of similarity of the experimental and theoretical SAXS profiles could be rejected (Table S2). This also indicated that the theoretical SAXS profiles using those representative model structures were insufficient to express the experimental SAXS profiles. In contrast, six representative model structures generated using

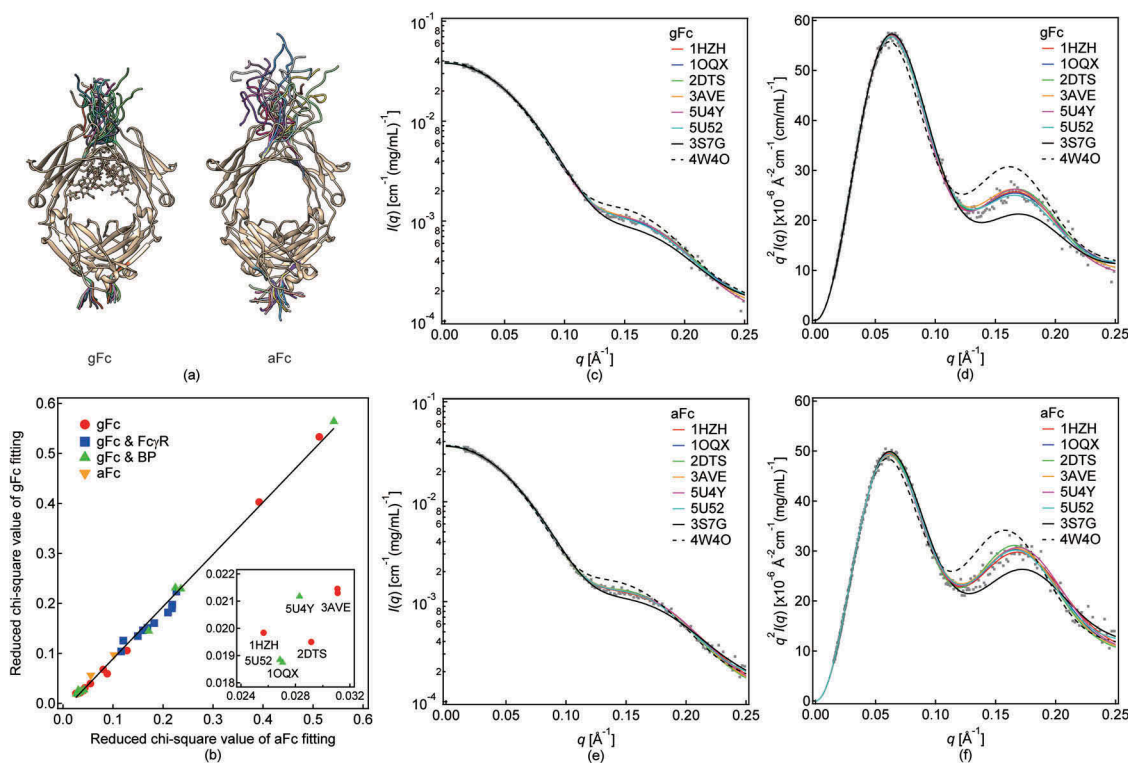


Figure 3. Homology modeling and fitting. (a) Ten example model structures of gFc (left) and aFc (right) calculated from the template structure of 1HZH. (b) A correlation plot of reduced chi-square values for 3 mg/mL SAXS profiles of gFc and aFc. BP denotes a binding protein. The black straight line represents the result of the regression analysis. The inset contains the plot of the lowest reduced chi-square value. (c–f) SAXS profiles with the lowest reduced chi-square values calculated based on five model structures. Log-linear plots (c, d) and Kratky plots (e, f) are shown. The gray dots indicate the experimentally determined SAXS profile of 3 mg/mL protein concentration.

the crystal structures of 1HZH, 1OQX, 2DTS, 3AVE, 5U4Y, and 5U52 had P -value above 0.01 for both gFc and aFc fitting, indicating that the null hypothesis (H_0) could not be rejected. In statistical analysis, failure to reject the null hypothesis (H_0) does not ascertain statistical similarity. Nevertheless, the theoretical SAXS profiles generated from those six representative model structures indeed all agreed very well with the experimental SAXS profiles (Figure 3(c-h)). Therefore, we concluded that those six representative model structures could indeed represent the experimental SAXS profiles, considering the best-fitted representative model structures.

To confirm the characteristics of the best-fitted representative model structures, we generated correlation plots of the reduced chi-square values and the right singular vectors of each principal component extracted by the SVD analysis described above (Figure 4). The right singular vector of the

first principal component, which reflected the open or closed orientation characteristics, showed an association with the reduced chi-square value of each representative model structure, while other principal components did not (Figure S6). The first right singular vectors of the best-fitted representative model structures were in the range of -0.123 to 0.053 (Table S2), and most of their C_{H2} domain orientations were classed as semi-closed. This indicated that the C_{H2} domain orientations in both gFc and aFc were almost identical.

Discussion

In this study, we experimentally determined the SAXS profiles of gFc and aFc to characterize their conformations in solution. The shapes of the experimentally determined SAXS profiles of gFc and aFc were similar, but also clearly different (Figure 1(a,b) and S2a-c). Interestingly, R_g of gFc was smaller than that of aFc, despite the larger molecular mass of gFc than aFc (Table S1). The reason for this inconsistency became clear after comparing their $P(r)$ (Figure 1(c) and S2d). We interpreted these observations to indicate that the difference in $P(r)$ between gFc and aFc was derived from the scattering from the N -linked glycan of gFc; that the intradomain conformation and the inter-domain orientation of polypeptide portions were equivalent; and that the change of the C_{H2} domain orientation in aFc caused by deglycosylation was small. To demonstrate that the presence of the N -linked glycan was sufficient to lead to the difference in the SAXS profiles of gFc and aFc, we further evaluated the structural characteristics in the experimentally determined SAXS profiles of gFc and aFc by performing a fitting analysis using theoretical SAXS profiles based on the existing Fc crystal structures (Figure 3 and S5). The data indicated that the measured SAXS profiles of both gFc and aFc were best-fitted using the theoretical SAXS profiles based on the common Fc crystal structure, which adopted a “semi-closed” C_{H2} domain orientation (Figure 4).

SAXS analysis of gFc and aFc was previously performed by Borrok *et al.*¹⁵ The authors found that R_g is larger in aFc than in gFc, and concluded that aFc forms an open orientation in solution. The SAXS analysis presented here reproduced the observation that R_g of aFc was larger than that of gFc (Figure 1 and Table S1), indicating that the divergent conclusions did not result from the differences of experimental conditions, e.g., sample preparation methods and the measuring equipment. The N -linked glycan of gFc is located near the center of the three-dimensional Fc structure, filling the hollow between the two C_{H2} domains. When the gFc and aFc structures are modeled as solid and hollow spheres, respectively, R_g of a solid sphere is smaller than that of a hollow sphere whose outer shell has the same diameter (see also SUPPLEMENTARY DISCUSSION).³⁷ Therefore, it is reasonable to assume that the scattering from the N -glycan reduces the R_g of gFc compared with aFc, without any changes in the C_{H2} domain orientation.

The analysis presented here provided information about the characteristics of an averaged conformation of gFc and aFc in solution, and we did not analyze a conformational distribution. As for the distribution, the previous study using RDC technique suggested that gFc has little conformational deviation in

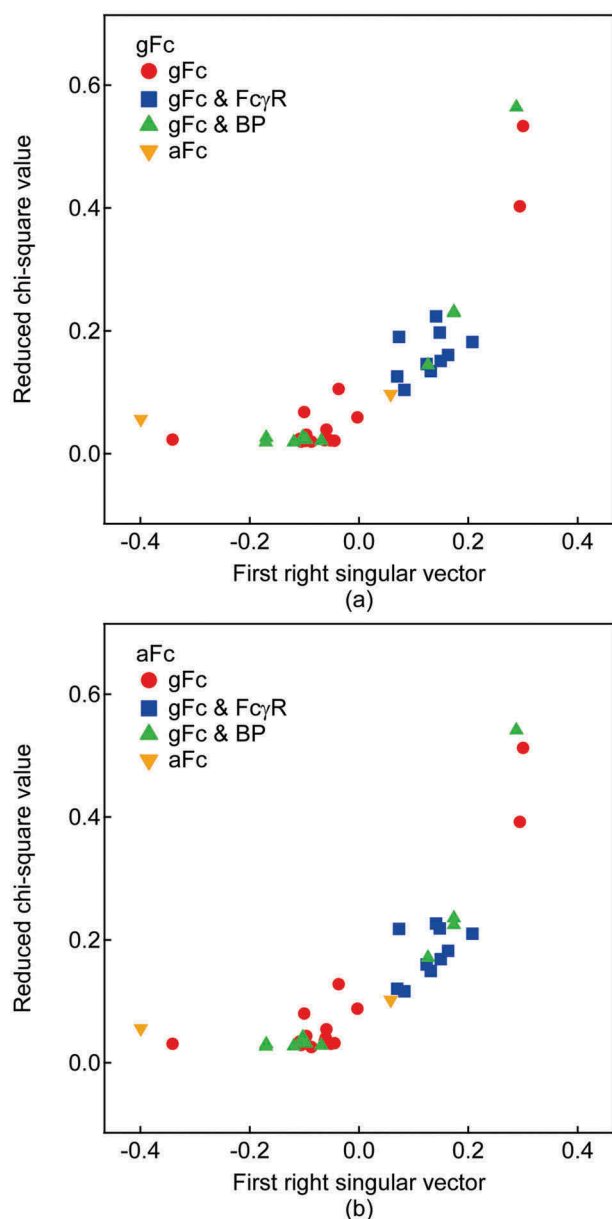


Figure 4. Correlation plots between the chi-square value for 3 mg/mL SAXS profiles and the first right singular vector; gFc (a) and aFc (b). BP denotes a binding protein.

solution.¹⁹ In contrast, Remesh *et al.* recently reported an obvious distribution in the C_{H2} domain orientation of gFc by combining atomistic modeling with experimental SAXS data in a multi-conformational analysis.²⁶ Their SAXS profile at pH 7.5 (SASDBD accession code: SASDDT4) is in excellent agreement with the SAXS profile in our study. The scattering curves measured by Remesh *et al.* were higher ($\sim 0.5 \text{ \AA}^{-1}$) than the scattering vectors in our experiment and they used these data to refine the characteristics of the local conformations including the N-terminal hinge, the N-linked glycan, the C_{H2}-C_{H3} linker, the C-terminal region, and the short flexible loop in the C_{H3} domain. They showed that the derived SAXS profiles can be best explained by the weighted sum of theoretical SAXS profiles composed of four dominant model structures with different C_{H2} domain orientations. To clarify the relevance between the findings of Remesh *et al.* and our analytical results, we overlaid their four model structures on the correlation plots of 40 crystal structure data (Figure S7). This showed that the four model structures fell in the range of the semi-closed C_{H2} domain orientation, and neither conformation was classified into either the closed or open conformations. This indicates that the distribution of gFc conformations is constrained within a relatively narrow conformational space, compared to the vast conformational space that includes the closed and open C_{H2} domain orientations. In addition, Yogo *et al.* detected the open orientation of gFc in complex with FcγRIIIb, in solution, using deuteration-assisted small-angle neutron scattering (SANS).³⁸ An important conclusion reported by the authors is that the experimental population of the semi-closed orientation and the open orientation, in complex with FcγRIIIb, was in agreement with the theoretical population of free and bound form, calculated based on the dissociation constant between gFc and FcγRIIIb. This suggests that the transition of the C_{H2} domain orientation in gFc from semi-closed to open would be governed by a classical induced-fit mechanism. Therefore, in solution and in the absence of FcγRIIIb, gFc would be expected to predominantly adopt the semi-closed orientation, within the narrow range of conformational distribution. As for the conformational distribution of aFc, recent studies employing molecular dynamics simulation and Förster resonance energy transfer (FRET) analyses proposed that deglycosylation increases the range of conformational distribution in the C_{H2} domain,^{30,33,39–41} although the characterization of the conformational distribution of aFc by SAXS has not been performed.

Deglycosylation of the Fc region causes a reduction of its binding affinity for FcγR.^{14,19,42–44} One hypothesis explaining this phenomenon involves alteration of the static C_{H2} domain orientation by deglycosylation,^{15–17} but the results of SAXS analysis presented in this study reasonably disproved it. Subedi *et al.* proposed that the conformational change in the C'E loop in the C_{H2} domain that results from deglycosylation is responsible for the reduced affinity to FcγRIIIa.¹⁹ The authors found that the magnitude of the chemical shifts of Y300 in the C'E loop in a range of Fc variants was strongly correlated with FcγRIIIa affinity. In addition, protein engineering approaches involving random amino acid replacement have succeeded in generating aFc variants with recovered FcγR affinity.^{3,5} Ju *et al.* performed single-molecular FRET analysis with one such aFc variant (Fc5), in which the FcγRI affinity was recovered by amino acid replacement in the

C_{H3} domain,^{45,46} and demonstrated that the restriction of the orientation and domain motion of the C_{H2} domain is critical for the recovery of FcγR affinity.³⁹ Combining the results of high-resolution analyses, such as SAXS and NMR, with the Fc variant repertoire that exhibits recovered affinity will contribute to further elucidation of the molecular mechanisms that underpin the reduced FcγR affinity associated with deglycosylation.

In conclusion, using SAXS, we proved that the removal of the N-linked-glycan from the Fc region only minimally perturbed the C_{H2} domain orientation. The pair-distance distribution function calculated from the experimentally determined SAXS profiles indicated that the conformational characteristics of the C_{H2} domain orientation between gFc and aFc, were equivalent. Further, comparison of the experimentally determined SAXS profiles and the theoretical SAXS profiles calculated based on the model structures revealed that both gFc and aFc adopted a “semi-closed” C_{H2} domain orientation in solution. These findings will guide the development of methodology for the production of highly refined functional Fc variants.

Materials and methods

Sample preparation

Glycosylated human IgG1 Fc region (gFc) was prepared by papain digestion, and the recombinant human aglycosylated IgG1 Fc region (aFc) was produced using the *Escherichia coli* expression system, as previously described.⁴⁷ The averaged molecular masses of the purified samples (> 95% monomeric) were determined and analyzed using Acquity UPLC I-Class and SYNAPT G2-Si systems (Waters, Millford, MA, USA) and the Expressionist Refiner MS software (GeneData, Basel, Switzerland), respectively (Figure S8 and Table S1). The mass spectrum of gFc revealed several peaks representing a repertoire of glycoforms (Figure S8a). The molecular mass of the main peak agreed with the theoretical molecular mass estimated based on the amino acid sequences of the two heavy chains (from T236 to G447) and the attached G0F/G1F glycan. The experimental information on the glycan was used for the construction of N-linked glycan template during homology modeling, as described later. Papain digestion occurred at the same position as previously reported.⁴⁸ The averaged molecular mass of aFc agreed with the theoretical molecular mass estimated for the D232–K448 fragment with an additional N-terminal alanine (Figure S8b). The formation of the interchain disulfide bridges in the hinge region of aFc has been confirmed in a previous study.⁴⁷ The original buffer in the purified protein samples (2–5 mg/mL) was exchanged to 20 mM citrate-phosphate buffer (pH 7.0) by dialysis.

SAXS

The SAXS analyses were performed using the beamline BL-10C at the Photon Factory (PF) of the High Energy Acceleration Research Organization (KEK; Tsukuba, Japan). The X-ray wavelength was 0.12 nm; the camera length (2028 mm) was

determined by using a scattering pattern of silver behenate as a standard.⁴⁹ X-ray scattering intensities were recorded using PILATUS 2M detector (Dectris, Baden-Daettwil, Switzerland). The temperature was controlled at $25.0 \pm 0.1^\circ\text{C}$; 15 images were collected for each sample; and each image was recorded during a 2-s exposure time. A circular one-dimensional average of the image was computed by the program *Nika*.⁵⁰ Additional SAXS measurement parameters⁵¹ are summarized in Table S1. Data processing procedure was described in SUPPLEMENTARY METHOD.

The scattering data collected using the BL-10C beamline are deposited in the Small Angle Scattering Biological Data Bank (SASBDB),⁵² under the following accession codes: SASDDG2 and SASDDH2.

SVD

Forty-two crystal structures of the human IgG Fc region (Table S2)^{17,18,30,53–75} were selected based on the information deposited in the UniProt Knowledgebase (accession number: P01857) and were obtained from PDB. All crystal structures of human IgG1 Fc region available in the PDB that satisfied the following criteria were selected: (a) the three-dimensional coordinates of the Ca atoms of each amino acid residue from S239 to S442 were completely assigned; (b) two heavy chains must be present in the crystal structure; (c) the structure represented a wild-type sequence without any amino acid substitutions. The dataset for SVD calculation was prepared as follows. First, because of the existence of unassigned amino acid residues in the N-terminal hinge and C-terminal regions of several crystal structures, the three-dimensional coordinates of Ca atoms of each amino acid residue between S239–S442 without the N-linked glycan were extracted from the original crystal structure of each Fc region. Next, the three-dimensional coordinates of Ca atoms in the C_H3 domain (G341–S442) were aligned using the Pymol software. Then, the deviation of the three-dimensional coordinates of each Ca atom in the 42 crystal structures was calculated by subtracting the averaged three-dimensional coordinates of each Ca atom. Finally, SVD was performed on the deviation dataset using LAPACK package in IGOR Pro (Wavemetrics, Portland, OR, USA).^{32,47,76,77}

Homology modeling and determination of theoretical SAXS profiles

The three-dimensional coordinates of amino acid residues in the N-terminal hinge region (gFc, T225–P238; aFc, the N-terminal alanine and D221–P238) and the C-terminal region (gFc, S441–G447; aFc, S441–K448) of the Fc region were predicted using the MODELLER program.^{78,79} The three-dimensional coordinates of all atoms between S239–S442 from the 42 Fc crystal structures were used as fixed template structures for calculating the model structure of aFc and gFc (Table S2). In the fixed template structure for aFc, the N-linked glycan was removed if it existed within the original coordinates. For the template structure of gFc, the three-dimensional coordinates of the N-linked glycan were reconstructed because they had not been completely

assigned in some of the original gFc crystal structures. In this study, we used the rigid N-linked glycan coordinates from a specific gFc crystal structure. Investigations using NMR revealed significant mobility of the N-linked glycan, such as α 1-3 and α 1-6Man branches, in solution.^{80,81} Meanwhile, the fitting analysis of the measured SAXS profile using the theoretical SAXS profiles from the pool of different modeled glycan structures revealed that the glycan filled the internal space between C_H2 domains.^{26,35} Based on these reports, we expected that the glycan would fill the internal space of the C_H2 domains in solution, and potential dynamics of glycans observed by NMR experiments would occur in the limited internal space. Thus, the rigid glycan coordinates used in this study was a valid option as a glycan model. In the template structure of gFc, the pair of G0F and G1F glycans (G0F/G1F) was selected as the N-linked glycan template, with reference to the three-dimensional coordinates of the N-linked glycan of a specific gFc crystal structure (PDB: 4BYH⁵⁸), by aligning the C_H2 domain (S239–K340) of 4BYH and that of each template structure. One hundred intact model structures were predicted for each of the 84 template structures of gFc and aFc. Two inter-chain disulfide bridges at the hinge region (C226 and C229) were introduced by using a manual restraint. Some of the intact model structures calculated based on the template structures for 1T89, 1H3V, 1H3Y, 3DO3, 3S7G, 4BYH, 4WI2, and 5U52, returned an unacceptable structure, in which the N-terminal hinge region penetrated the DE loop of the C_H2 domain. For 1T89, 3DO3, and 5U52, unacceptable structures were not computed frequently. The unacceptable structures were manually replaced with the accepted structures with the non-penetrated hinge region. For 3S7G, 4BYH, and 4WI2, the unacceptable structure accounted for the majority of output. The population of the unacceptable structures was reduced by adding one or more N-terminal amino acid residues to the fixed template structures; the unacceptable structures were then replaced with accepted ones. For 1H3V and 1H3Y, the unacceptable structure also accounted for the majority of structures, but the population of the unacceptable structures could not be reduced using the described procedure. Therefore, the intact model structures for 1H3V and 1H3Y were excluded from further analysis. Consequently, 40 crystal structures and 80 template structures were included in analysis. SAXS profiles of each model structure and the fitting analysis in the q range of 0.015 to 0.250 \AA^{-1} was performed using the Crysol software.²³ The fitting results were evaluated based on the reduced chi-square value and the P -value using the pair-wise correlation map (CorMap) analysis in the DATCMP program within the ATSAS software.^{23,36,82}

Acknowledgments

This study was partially supported by the Japan Agency for Medical Research and Development (AMED; grant no. JP17ae0101003). The SAXS experiment was performed with the approval of the Photon Factory Program Advisory Committee (proposal no. 2015G061).

Disclosure of Potential Conflicts of Interest

No potential conflicts of interest were disclosed.

Funding

This work was supported by the Japan Agency for Medical Research and Development [JP17ae0101003].

Abbreviations

aFc	aglycosylated Fc region;
BP	binding protein;
D_{\max}	maximum distance;
Fc	crystallizable fragment;
Fc γ R	Fc gamma receptor;
gFc	glycosylated Fc region;
IgG	immunoglobulin G;
NMR	nuclear magnetic resonance;
PCA	principal component analysis;
PDB	Protein Data Bank;
RDC	residual dipolar coupling;
R_g	radius of gyration;
SAXS	small-angle X-ray scattering;
SVD	singular value decomposition

ORCID

Hiroshi Imamura <http://orcid.org/0000-0001-8924-747X>

Risa Shibuya <http://orcid.org/0000-0002-1337-9334>

Shinya Honda <http://orcid.org/0000-0002-7878-3944>

References

- Shepard H, Phillips G, Thanos C, Feldmann M. Developments in therapy with monoclonal antibodies and related proteins. *Clin Med*. 2017;17(3):220–232. doi:10.7861/clinmedicine.17-3-220.
- Elvin J, Couston R, van der Walle C. Therapeutic antibodies: market considerations, disease targets and bioprocessing. *Int J Pharm*. 2013;440(1):83–98. doi:10.1016/j.ijpharm.2011.12.039.
- Ju M, Jung S. Aglycosylated full-length IgG antibodies: steps toward next-generation immunotherapeutics. *Curr Opin Biotechnol*. 2014;30:128–139. doi:10.1016/j.copbio.2014.06.013.
- Hristodorov D, Fischer R, Linden L. With or without sugar? (A) glycosylation of therapeutic antibodies. *Mol Biotechnol*. 2013;54(3):1056–1068. doi:10.1007/s12033-012-9612-x.
- Jung S, Kang T, Kelton W, Georgiou G. Bypassing glycosylation: engineering aglycosylated full-length IgG antibodies for human therapy. *Curr Opin Biotechnol*. 2011;22(6):858–867. doi:10.1016/j.copbio.2011.03.002.
- Spadiut O, Capone S, Krainer F, Glieder A, Herwig C. Microbials for the production of monoclonal antibodies and antibody fragments. *Trends Biotechnol*. 2014;32(1):54–60. doi:10.1016/j.tibtech.2013.10.002.
- Frenzel A, Hust M, Schirrmann T. Expression of recombinant antibodies. *Front Immunol*. 2013;4. doi:10.3389/fimmu.2013.00217.
- Fang J, Richardson J, Du Z, Zhang Z. Effect of Fc-glycan structure on the conformational stability of IgG revealed by hydrogen/deuterium exchange and limited proteolysis. *Biochemistry*. 2016;55(6):860–868. doi:10.1021/acs.biochem.5b01323.
- Hristodorov D, Fischer R, Joerissen H, Muller-Tiemann B, Apeler H, Linden L. Generation and comparative characterization of glycosylated and aglycosylated human IgG1 antibodies. *Mol Biotechnol*. 2013;53(3):326–335. doi:10.1007/s12033-012-9531-x.
- Alsenaidy M, Kim J, Majumdar R, Weis D, Joshi S, Tolbert T, Russell Middaugh C, Volkin DB. High-throughput biophysical analysis and data visualization of conformational stability of an IgG1 monoclonal antibody after deglycosylation. *J Pharm Sci*. 2013;102(11):3942–3956. doi:10.1002/jps.23730.
- Kayser V, Chennamsetty N, Voynov V, Forrer K, Helk B, Trout B. Glycosylation influences on the aggregation propensity of therapeutic monoclonal antibodies. *Biotechnol J*. 2011;6(1):38–44. doi:10.1002/biot.201000091.
- Zheng K, Bantog C, Bayer R. The impact of glycosylation on monoclonal antibody conformation and stability. *MAbs*. 2011;3(6):568–576. doi:10.4161/mabs.3.6.17922.
- Mimura Y, Church S, Ghirlando R, Ashton P, Dong S, Goodall M, Lund J, Jefferis R. The influence of glycosylation on the thermal stability and effector function expression of human IgG1-Fc: properties of a series of truncated glycoforms. *Mol Immunol*. 2000;37(12–13):697–706. doi:10.1016/S0161-5890(00)00105-X.
- Jefferis R. Recombinant antibody therapeutics: the impact of glycosylation on mechanisms of action. *Trends Pharmacol Sci*. 2009;30(7):356–362. doi:10.1016/j.tips.2009.04.007.
- Borrok MJ, Jung ST, Kang TH, Monzingo AF, Georgiou G. Revisiting the role of glycosylation in the structure of human IgG Fc. *ACS Chem Biol*. 2012;7(9):1596–1602. doi:10.1021/cb300130k.
- Feige M, Nath S, Catharino S, Weinfurter D, Steinbacher S, Buchner J. Structure of the murine unglycosylated IgG1 Fc fragment. *J Mol Biol*. 2009;391(3):599–608. doi:10.1016/j.jmb.2009.06.048.
- Krapp S, Mimura Y, Jefferis R, Huber R, Sondermann P. Structural analysis of human IgG-Fc glycoforms reveals a correlation between glycosylation and structural integrity. *J Mol Biol*. 2003;325(5):979–989. doi:10.1016/S0022-2836(02)01250-0.
- Kiyoshi M, Caaveiro JM, Kawai T, Tashiro S, Ide T, Asaoka Y, Hatayama K, Tsumoto K. Structural basis for binding of human IgG1 to its high-affinity human receptor Fc γ RI. *Nat Commun*. 2015;6:6866. doi:10.1038/ncomms7866.
- Subedi G, Barb A. The structural role of antibody N-Glycosylation in receptor interactions. *Structure*. 2015;23(9):1573–1583. doi:10.1016/j.str.2015.06.015.
- Idusogie EE, Presta LG, Gazzano-Santoro H, Totpal K, Wong PY, Ultsch M, Meng YG, Mulkerrin MG. Mapping of the C1q binding site on rituxan, a chimeric antibody with a human IgG1 Fc. *J Immunol*. 2000;164(8):4178–4184. doi:10.4049/jimmunol.164.8.4178.
- Hammel M. Validation of macromolecular flexibility in solution by small-angle X-ray scattering (SAXS). *Eur Biophys J*. 2012;41(10):789–799. doi:10.1007/s00249-012-0820-x.
- Svergun DI, Koch MHJ, Timmins PA, May RP. Small angle X-ray and neutron scattering from solutions of biological macromolecules. Oxford (UK): Oxford University Press; 2013.
- Svergun D, Barberato C, Koch M. CRYSOLE - A program to evaluate x-ray solution scattering of biological macromolecules from atomic coordinates. *J Appl Crystallogr*. 1995;28:768–773. doi:10.1107/S0021889895007047.
- Sumi T, Imamura H, Morita T, Isogai Y, Nishikawa K. Model-potential-free analysis of small angle scattering of proteins in solution: insights into solvent effects on protein-protein interaction. *Phys Chem Chem Phys*. 2014;16(46):25492–25497. doi:10.1039/c4cp03606a.
- Imamura H, Morita T, Sumi T, Isogai Y, Kato M, Nishikawa K. Modulation of the intermolecular interaction of myoglobin by removal of the heme. *J Synchrotron Radiat*. 2013;20(6):919–922. doi:10.1107/S0909049513022772.
- Remesh SG, Armstrong AA, Mahan AD, Luo J, Hammel M. Conformational plasticity of the immunoglobulin Fc domain in solution. *Structure*. 2018;26(7):1007–1014.e2. doi:10.1016/j.str.2018.03.017.
- Daniel F, Alexey GK, Dmitri IS. Automated acquisition and analysis of small angle X-ray scattering data. *Nucl Instrum Meth Phys Res A*. 2012;689:52–59. doi:10.1016/j.nima.2012.06.008.
- Glatter O, Kratky O. Small angle X-ray scattering. London (UK): Academic Press; 1982.

29. Semisotnov GV, Kihara H, Kotova NV, Kimura K, Amemiya Y, Wakabayashi K, Serdyuk IN, Timchenko AA, Chiba K, Nikaido K, et al. Protein globularization during folding. A study by synchrotron small-angle X-ray scattering. *J Mol Biol.* 1996;262(4):559–574. doi:10.1006/jmbi.1996.0535.
30. Frank M, Walker RC, Lanzilotta WN, Prestegard JH, Barb AW. Immunoglobulin G1 Fc domain motions: implications for Fc engineering. *J Mol Biol.* 2014;426(8):1799–1811. doi:10.1016/j.jmb.2014.01.011.
31. Stein SAM, Loccisano AE, Firestine SM, Evansck JD. Principal components analysis: a review of its application on molecular dynamics data. *Annu Rep Comput Chem.* 2006;2:233–261. doi:10.1016/S1574-1400(06)02013-5.
32. Hendler RW, Shrager RI. Deconvolutions based on singular value decomposition and the pseudoinverse: a guide for beginners. *J Biochem Biophys Methods.* 1994;28(1):1–33. doi:10.1016/0165-022X(94)90061-2.
33. Zhang Y. Understanding the impact of Fc glycosylation on its conformational changes by molecular dynamics simulations and bioinformatics. *Mol Biosyst.* 2015;11(12):3415–3424. doi:10.1039/c5mb00602c.
34. Houde D, Arndt J, Domeier W, Berkowitz S, Engen JR. Characterization of IgG1 conformation and conformational dynamics by hydrogen/deuterium exchange mass spectrometry. *Anal Chem.* 2009;81(14):5966. doi:10.1021/ac9009287.
35. Guttman M, Weinkam P, Sali A, Lee KK. All-atom ensemble modeling to analyze small-angle X-ray scattering spectra. *Nat Methods.* 2015;12(5):419–422. doi:10.1016/j.str.2013.02.004.
36. Franke D, Jeffries CM, Svergun DI. Correlation Map, a goodness-of-fit test for one-dimensional X-ray scattering spectra. *Nat Methods.* 2015;12(5):419–422. doi:10.1038/nmeth.3358.
37. Feigin LA, Svergun DI, Taylor GW. *Structure Analysis by small-angle X-ray and neutron scattering.* Berlin (Germany): Springer; 1987.
38. Yogo R, Yanaka S, Yagi H, Martel A, Porcar L, Ueki Y, Inoue R, Sato N, Sugiyama M, Kato K. Characterization of conformational deformation-coupled interaction between immunoglobulin G1 Fc glycoprotein and a low-affinity Fcγ receptor by deuteration-assisted small-angle neutron scattering. *Biochem Biophys Rep.* 2017;12:1–4. doi:10.1016/j.bbrep.2017.08.004.
39. Ju M, Na J, Yu Y, Kim J, Jeong C, Jung S. Structural consequences of aglycosylated IgG Fc variants evolved for Fc gamma RI binding. *Mol Immunol.* 2015;67(2):350–356. doi:10.1016/j.molimm.2015.06.020.
40. Piraino M, Kelliher M, Aburas J, Southern C. Single molecule Forster resonance energy transfer studies of the effect of EndoS deglycosylation on the structure of IgG. *Immunol Lett.* 2015;167(1):29–33. doi:10.1015/j.imlet.2015.06.011.
41. Kelliher M, Jacks R, Piraino M, Southern C. The effect of sugar removal on the structure of the Fc region of an IgG antibody as observed with single molecule Forster Resonance Energy Transfer. *Mol Immunol.* 2014;60(2):103–108. doi:10.1016/j.molimm.2014.04.005.
42. Lux A, Yu X, Scanlan C, Nimmerjahn F. Impact of immune complex size and glycosylation on IgG binding to human Fc gamma Rs. *J Immunol.* 2013;190(8):4315–4323. doi:10.4049/jimmunol.1200501.
43. Simmons L, Reilly D, Klimowski L, Raju T, Meng G, Sims P, Hong K, Shields RL, Damico LA, Rancatore P, et al. Expression of full-length immunoglobulins in *Escherichia coli*: rapid and efficient production of aglycosylated antibodies. *J Immunol Methods.* 2002;263(1–2):133–147. doi:10.1016/S0022-1759(02)00036-4.
44. Mimura Y, Sondermann P, Ghirlando R, Lund J, Young S, Goodall M, Jefferis R. Role of oligosaccharide residues of IgG1-Fc in Fc gamma RIIb binding. *J Biol Chem.* 2001;276(49):45539–45547. doi:10.1074/jbc.M107478200.
45. Jung S, Kang T, Kim D. Engineering an aglycosylated Fc variant for enhanced Fc gamma RI engagement and pH-dependent human FcRn binding. *Biotechnol Bioprocess Eng.* 2014;19(5):780–789. doi:10.1007/s12257-013-0432-z.
46. Jung S, Reddy S, Kang T, Borrok M, Sandlie I, Tucker P, Georgiou G. Aglycosylated IgG variants expressed in bacteria that selectively bind Fc gamma RI potentiate tumor cell killing by monocyte-dendritic cells. *Proc Natl Acad Sci U S A.* 2010;107(2):604–609. doi:10.1073/pnas.0908590107.
47. Yageta S, Shibuya R, Imamura H, Honda S. Conformational and colloidal stabilities of human immunoglobulin G Fc and its cyclized variant: independent and compensatory participation of domains in aggregation of multidomain proteins. *Mol Pharm.* 2017;14(3):699–711. doi:10.1021/acs.molpharmaceut.6b00983.
48. Wang A, Wang I. Cleavage sites of human IgG1 immunoglobulin by papain. *Immunochemistry.* 1977;14(3):197–200. doi:10.1016/0019-2791(77)90194-X.
49. Huang T, Toraya H, Blanton T, Wu Y. X-ray powder diffraction analysis of silver behenate, a possible low-angle diffraction standard. *J Appl Crystallogr.* 1993;26:180–184. doi:10.1107/S0021889892009762.
50. Ilavsky J. Nika: software for two-dimensional data reduction. *J Appl Crystallogr.* 2012;45:324–328. doi:10.1107/S0021889812004037.
51. Trewhella J, Duff AP, Durand D, Gabel F, Guss JM, Hendrickson WA, Hura GL, Jacques DA, Kirby NM, Kwan AH, et al. 2017 publication guidelines for structural modelling of small-angle scattering data from biomolecules in solution: an update. *Acta Crystallogr D Struct Biol.* 2017;73:710–728. doi:10.1107/S2059798317011597.
52. Valentini E, Kikhney AG, Previtali G, Jeffries CM, Svergun DI. SASBDB, a repository for biological small-angle scattering data. *Nucleic Acids Res.* 2015;43(Databaseissue):D357–63. doi:10.1093/nar/gku1047.
53. Deisenhofer J. Crystallographic refinement and atomic models of a human Fc fragment and its complex with fragment B of protein A from *Staphylococcus aureus* at 2.9- and 2.8-Å resolution. *Biochemistry.* 1981;20(9):2361–2370. doi:10.1021/bi00512a001.
54. Saphire EO, Parren PW, Pantophlet R, Zwick MB, Morris GM, Rudd PM, Dwek RA, Stanfield RL, Burton DR, Wilson IA. Crystal structure of a neutralizing human IGG against HIV-1: a template for vaccine design. *Science.* 2001;293(5532):1155–1159. doi:10.1126/science.1061692.
55. Matsumiya S, Yamaguchi Y, Saito J, Nagano M, Sasakawa H, Otaki S, Satoh M, Shitara K, Kato K. Structural comparison of fucosylated and nonfucosylated Fc fragments of human immunoglobulin G1. *J Mol Biol.* 2007;368(3):767–779. doi:10.1016/j.jmb.2007.02.034.
56. Crispin M, Bowden TA, Coles CH, Harlos K, Aricescu AR, Harvey DJ, Stuart DI, Jones EY. Carbohydrate and domain architecture of an immature antibody glycoform exhibiting enhanced effector functions. *J Mol Biol.* 2009;387(5):1061–1066. doi:10.1016/j.jmb.2009.02.033.
57. Sibérel S, Ménez R, Jorieux S, de Romeuf C, Bourel D, Fridman WH, Ducancel F, Stura EA, Teillaud J-L. Effect of zinc on human IgG1 and its FcγR interactions. *Immunol Lett.* 2012;143(1):60–69. doi:10.1016/j.imlet.2012.02.002.
58. Crispin M, Yu X, Bowden TA. Crystal structure of sialylated IgG Fc: implications for the mechanism of intravenous immunoglobulin therapy. *Proc Natl Acad Sci U S A.* 2013;110(38):E3544–6. doi:10.1073/pnas.1310657110.
59. Silva-Martín N, Bartual SG, Ramírez-Aportela E, Chacón P, Park CG, Hermoso JA. Structural basis for selective recognition of endogenous and microbial polysaccharides by macrophage receptor SIGN-R1. *Structure.* 2014;22(11):1595–1606. doi:10.1016/j.str.2014.09.001.
60. Ahmed AA, Giddens J, Pincetic A, Lomino JV, Ravetch JV, Wang LX, Bjorkman PJ. Structural characterization of anti-inflammatory immunoglobulin G Fc proteins. *J Mol Biol.* 2014;426(18):3166–3179. doi:10.1016/j.jmb.2014.07.006.
61. Chen CL, Hsu JC, Lin CW, Wang CH, Tsai MH, Wu CY, Wong C-H, Ma C. Crystal structure of a homogeneous IgG-Fc glycoform with the N-glycan designed to maximize the antibody dependent cellular cytotoxicity. *ACS Chem Biol.* 2017;12(5):1335–1345. doi:10.1021/acscchembio.7b00140.
62. Sondermann P, Huber R, Oosthuizen V, Jacob U. The 3.2-Å crystal structure of the human IgG1 Fc fragment-Fc gammaRIII complex. *Nature.* 2000;406(6793):267–273. doi:10.1038/35018508.
63. Radaev S, Motyka S, Fridman WH, Sautes-Fridman C, Sun PD. The structure of a human type III Fc gamma receptor in complex

- with Fc. *J Biol Chem.* 2001;276(19):16469–16477. doi:10.1074/jbc.M100350200.
64. Mizushima T, Yagi H, Takemoto E, Shibata-Koyama M, Isoda Y, Iida S, Masuda K, Satoh M, Kato K. Structural basis for improved efficacy of therapeutic antibodies on defucosylation of their Fc glycans. *Genes Cells.* 2011;16(11):1071–1080. doi:10.1111/j.1365-2443.2011.01552.x.
65. Ramsland PA, Farrugia W, Bradford TM, Sardjono CT, Esparon S, Trist HM, Powell MS, Tan PS, Cendron AC, Wines BD, et al. Structural basis for Fc gammaRIIa recognition of human IgG and formation of inflammatory signaling complexes. *J Immunol.* 2011;187(6):3208–3217. doi:10.4049/jimmunol.1101467.
66. Ferrara C, Grau S, Jäger C, Sondermann P, Brünker P, Waldhauer I, Hennig M, Ruf A, Rufer AC, Stihle M, et al. Unique carbohydrate-carbohydrate interactions are required for high affinity binding between Fc gammaRIII and antibodies lacking core fucose. *Proc Natl Acad Sci U S A.* 2011;108(31):12669–12674. doi:10.1073/pnas.1108455108.
67. Lu J, Chu J, Zou Z, Hamacher NB, Rixon MW, Sun PD. Structure of FcγRI in complex with Fc reveals the importance of glycan recognition for high-affinity IgG binding. *Proc Natl Acad Sci U S A.* 2015;112(3):833–838. doi:10.1073/pnas.1418812112.
68. Oganessian V, Mazor Y, Yang C, Cook KE, Woods RM, Ferguson A, Bowen MA, Martin T, Zhu J, Wu H, et al. Structural insights into the interaction of human IgG1 with FcγRI: no direct role of glycans in binding. *Acta Crystallogr D Biol Crystallogr.* 2015;71(Pt 11):2354–2361. doi:10.1107/S1399004715018015.
69. DeLano WL, Ultsch MH, de Vos AM, Wells JA. Convergent solutions to binding at a protein-protein interface. *Science.* 2000;287(5456):1279–1283. doi:10.1126/science.287.5456.1279.
70. Sauer-Eriksson AE, Kleywegt GJ, Uhlén M, Jones TA. Crystal structure of the C2 fragment of streptococcal protein G in complex with the Fc domain of human IgG. *Structure.* 1995;3(3):265–278. doi:10.1016/S0969-2126(01)00157-5.
71. Sprague ER, Wang C, Baker D, Bjorkman PJ. Crystal structure of the HSV-1 Fc receptor bound to Fc reveals a mechanism for antibody bipolar bridging. *PLoS Biol.* 2006;4(6):e148. doi:10.1371/journal.pbio.0040148.
72. James LC, Keeble AH, Khan Z, Rhodes DA, Trowsdale J. Structural basis for PRYSPRY-mediated tripartite motif (TRIM) protein function. *Proc Natl Acad Sci U S A.* 2007;104(15):6200–6205. doi:10.1073/pnas.0609174104.
73. Duquerroy S, Stura EA, Bressanelli S, Fabiane SM, Vaney MC, Beale D, Hamon M, Casali P, Rey FA, Sutton BJ, et al. Crystal structure of a human autoimmune complex between IgM rheumatoid factor RF61 and IgG1 Fc reveals a novel epitope and evidence for affinity maturation. *J Mol Biol.* 2007;368(5):1321–1331. doi:10.1016/j.jmb.2007.02.085.
74. Watanabe H, Honda S. Adaptive assembly: maximizing the potential of a given functional peptide with a tailor-made protein scaffold. *Chem Biol.* 2015;22(9):1165–1173. doi:10.1016/j.chembiol.2015.07.015.
75. Ultsch M, Braisted A, Maun HR, Eigenbrot C. 3-2-1: structural insights from stepwise shrinkage of a three-helix Fc-binding domain to a single helix. *Protein Eng Des Sel.* 2017;30(9):619–625. doi:10.1093/protein/gzx029.
76. Yageta S, Lauer T, Trout B, Honda S. Conformational and colloidal stabilities of isolated constant domains of human immunoglobulin G and their impact on antibody aggregation under acidic conditions. *Mol Pharm.* 2015;12(5):1443–1455. doi:10.1021/mp500759p.
77. Honda S, Yamasaki K, Sawada Y, Morii H. 10 residue folded peptide designed by segment statistics. *Structure.* 2004;12(8):1507–1518. doi:10.1016/j.str.2004.05.022.
78. Webb B, Sali A. Protein structure modeling with MODELLER. *Methods Mol Biol.* 2017;1654:39–54. doi:10.1007/978-1-4939-7231-9_4.
79. Webb B, Sali A. Comparative protein structure modeling using MODELLER. *Curr Protoc Bioinformatics.* 2014;47:5.6.1–32. doi:10.1002/0471250953.bi0506s47.
80. Barb AW, Prestegard JH. NMR analysis demonstrates immunoglobulin G N-glycans are accessible and dynamic. *Nat Chem Biol.* 2011;7(3):143–153. doi:10.1038/nchembio.511.
81. Barb AW, Meng L, Gao Z, Johnson RW, Moremen KW, Prestegard JH. NMR Characterization of immunoglobulin G Fc glycan motion on enzymatic sialylation. *Biochemistry.* 2012;51(22):4618–4626. doi:10.1021/bi300319q.
82. Franke D, Petoukhov MV, Konarev PV, Panjkovich A, Tuukkanen A, Mertens HDT, Kikhney AG, Hajizadeh NR, Franklin JM, Jeffries CM, et al. A comprehensive data analysis suite for small-angle scattering from macromolecular solutions. *J Appl Crystallogr.* 2017;50(4):1212–1225. doi:10.1107/S1600576717007786.